nature physics

LETTERS

PUBLISHED ONLINE: 18 APRIL 2016 | DOI: 10.1038/NPHYS3730

Charge density wave order in 1D mirror twin boundaries of single-layer $MoSe_2$

Sara Barja[1,2★†], Sebastian Wickenburg[1,2†], Zhen-Fei Liu[1,2], Yi Zhang[3,4], Hyejin Ryu[3], Miguel M. Ugeda[5,6,7], Zahid Hussain[3], Zhi-Xun Shen[8], Sung-Kwan Mo[3], Ed Wong[1,2], Miquel B. Salmeron[2,5,9], Feng Wang[2,5,10], Michael F. Crommie[2,5,10], D. Frank Ogletree[1,2★], Jeffrey B. Neaton[1,2,5,10] and Alexander Weber-Bargioni[1,2★]

We provide direct evidence for the existence of isolated, one-dimensional charge density waves at mirror twin boundaries (MTBs) of single-layer semiconducting $MoSe_2$. Such MTBs have been previously observed by transmission electron microscopy and have been predicted to be metallic in $MoSe_2$ and MoS_2[1–7]. Our low-temperature scanning tunnelling microscopy/spectroscopy measurements revealed a substantial bandgap of 100 meV opening at the Fermi energy in the otherwise metallic one-dimensional structures. We found a periodic modulation in the density of states along the MTB, with a wavelength of approximately three lattice constants. In addition to mapping the energy-dependent density of states, we determined the atomic structure and bonding of the MTB through simultaneous high-resolution non-contact atomic force microscopy. Density functional theory calculations based on the observed structure reproduced both the gap opening and the spatially resolved density of states.

Properties of two-dimensional (2D) transition metal dichalcogenides (TMDs) are highly sensitive to the presence of defects, and a detailed understanding of their structure may lead to tailoring of material properties through 'defect engineering'. Intrinsic defects have been studied extensively in graphene[8–12]. Defects in 2D semiconductors have been explored to a lesser extent, but are expected to substantially modify material properties. 2D TMD semiconductors are particularly interesting because they exhibit direct bandgaps in the visible range[13–15], high charge-carrier mobility[16,17], extraordinarily enhanced light–matter interactions[18–21] and potential applications in novel optoelectronic devices[22,23]. Individual atomic-scale defects in 2D TMDs are expected to modify charge transport[24] or introduce ferromagnetism[25], whereas one-dimensional defects such as grain boundaries and edges may alter electronic[1] and optical properties[1,26], and introduce magnetic[27] or catalytic[28,29] functionality.

Here we report the direct observation of one-dimensional (1D) charge density waves (CDWs) intrinsic to the conducting MTBs of monolayer $MoSe_2$. A 1D CDW is a macroscopic quantum state, where atoms in a 1D metallic system relax and break translational symmetry to reduce total energy by opening a small bandgap at the Fermi energy (E_F) and modulating the charge density at the periodicity of the lattice distortion[30,31]. Although CDW order has been observed in 2D TMD metals such as $NbSe_2$ and $TiSe_2$ at low temperature[32,33], CDWs have not previously been associated with 2D TMD semiconductors.

Most studies of 1D CDWs have been performed on ensembles of CDWs in conducting polymers, quasi-one-dimensional metals or self-assembled atomic chains adsorbed on semiconducting surfaces, where inter-CDW coupling can significantly impact CDW properties[34–38]. The CDWs observed here are electronically isolated from one another, and have truly one-dimensional character, forming an atomically precise model system to explore intrinsic CDW phenomena. We observed CDWs along 1D networks of MTBs in monolayer crystals of $MoSe_2$ grown by molecular beam epitaxy. Various morphologies have been proposed for MTBs in 2D semiconductors[1–4,6,7], and scanning tunnelling microscopy (STM) experiments have identified 1D metallic wires along boundaries in single-layer $MoSe_2$[5,39]. Our combined STM and non-contact atomic force microscopy (nc-AFM) studies have confirmed that these 1D wires are in fact MTBs.

We used low-temperature (4.5 K) scanning tunnelling microscopy/spectroscopy (STM/STS) to detect the CDW bandgap along MTBs in single-layer $MoSe_2$ and to spatially map the charge density modulations. We found that the MTB CDW was intrinsic to $MoSe_2$, and independent of substrate coupling. We determined the atomic structure of the MTB with parallel high-resolution nc-AFM. On the basis of this MTB structural model, we investigated the electronic structure by first-principles density functional theory (DFT) calculations. The calculated local density of states (LDOS) for the CDW reproduced the experimental STS spectra and charge density maps.

Figure 1a shows a high-resolution STM image of single-layer $MoSe_2$ grown by molecular beam epitaxy on bilayer graphene (BLG) on SiC(0001). Sharply defined pairs of identical parallel lines decorate the $MoSe_2$ monolayer. These bright lines have previously

[1]Molecular Foundry, Lawrence Berkeley National Laboratory, California 94720, USA. [2]Materials Sciences Division, Lawrence Berkeley National Laboratory, California 94720, USA. [3]Advanced Light Source, Lawrence Berkeley National Laboratory, Berkeley, California 94720, USA. [4]National Laboratory of Solid State Microstructures, School of Physics, Collaborative Innovation Center of Advanced Microstructures, Nanjing University, Nanjing 210093, China. [5]Department of Physics, University of California at Berkeley, Berkeley, California 94720, USA. [6]CIC nanoGUNE, Donostia-San Sebastián 20018, Spain. [7]Ikerbasque, Basque Foundation for Science, Bilbao 48013, Spain. [8]Stanford Institute of Materials and Energy Sciences, SLAC National Accelerator Laboratory, Menlo Park, California 94025, USA. [9]Department of Materials Science and Engineering, University of California Berkeley, California 94720, USA. [10]Kavli Energy NanoSciences Institute at the University of California Berkeley and the Lawrence Berkeley National Laboratory, Berkeley, California 94720, USA. †These authors contributed equally to this work. ★e-mail: sbarja@lbl.gov; dfogletree@lbl.gov; afweber-bargioni@lbl.gov

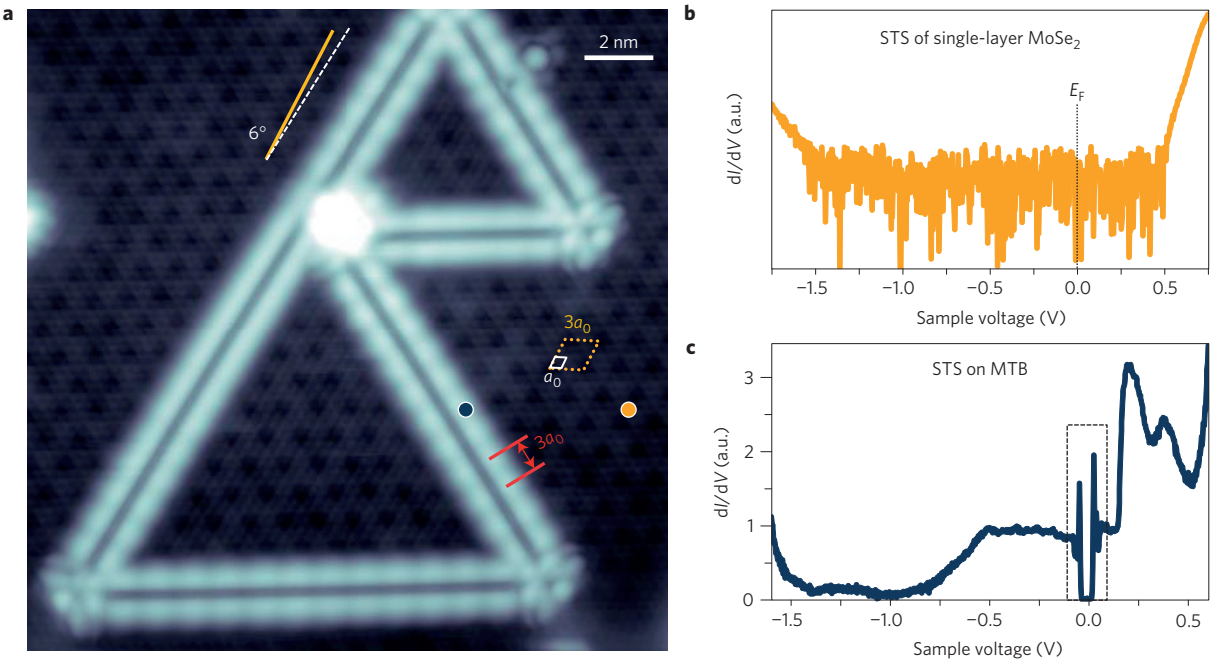

Figure 1 | Morphology and electronic structure of mirror twin boundaries in monolayer $MoSe_2$. a, High-resolution STM image of single-layer $MoSe_2$ on bilayer graphene ($V_s = -1.3$ V, $I_t = 20$ pA, $T = 4.5$ K) showing a 3 × 3 moiré pattern (dashed yellow line, with a single unit cell shown in white) and a modulation of the electronic states near the MTB with a wavelength of $3a_0$. There is a 6° misalignment between the moiré lattice (solid yellow line) and the MTB direction, determined by the $MoSe_2$ atomic lattice (dashed white line). **b**,**c**, Typical STM dI/dV spectra acquired on pristine monolayer $MoSe_2$/BLG (**b**; yellow dot in **a**) and on a mirror twin boundary (**c**; blue dot in **a**) show that the MTB has states throughout the semiconducting gap of monolayer $MoSe_2$. The dashed box in **c** indicates a bandgap opened around the Fermi level, E_F.

been described as inversion domain boundaries[5]. The apparent height of these features depends strongly on the bias applied between tip and sample, showing that the STM contrast originates primarily from the locally modified electronic structure rather than from topographic features. The contrast of the MTBs was modulated along their lengths with an average modulation period of 0.98 ± 0.05 nm, equivalent to 2.99 ± 0.15 lattice constants of $MoSe_2$.

The contrast modulation observed by STM has previously been attributed to a superlattice potential induced by the nearly commensurate 3 × 3 moiré pattern that forms when a monolayer of $MoSe_2$ is atomically aligned with its graphite growth substrate[5]. We are able to rule out this explanation for four reasons. First, we observed moiré pattern periodicities of 2.0, 2.6 and 3.0 lattice constants as a result of different TMD–graphene registries, whereas the MTB charge modulation ranged from 2.8 to 3.3 lattice constants (Fig. 1 and Supplementary Fig. 1). Second, we observed angles of up to 20 degrees between the moiré pattern and the MTB direction. This misalignment would break the symmetry of the electronic structure across the MTB, leading to uneven contrast between the two parallel lines, which we did not observe (Supplementary Fig. 1a). Third, we occasionally observed MTBs in second-layer islands of $MoSe_2$ with CDW modulation similar to the monolayer case, even though the first $MoSe_2$ layer screened the second layer from the graphene potential (Supplementary Fig. 2a,b). Last, we observed MTBs crossing step edges between single- and bilayer graphene (Supplementary Fig. 2c). The MTB charge modulation was unaltered, even though the change in dielectric screening between single- and bilayer graphene was sufficient to alter the semiconducting gap of single-layer $MoSe_2$[21]. Hence, we conclude that the MTB charge modulations we observed do not result from interactions with the graphene substrate, but rather are intrinsic properties of $MoSe_2$ MTBs.

To explore the origin of the charge modulation we measured and mapped the $MoSe_2$ LDOS using STM dI/dV spectroscopy. Figure 1b shows a dI/dV spectrum from monolayer $MoSe_2$ away from the MTB, with an electronic bandgap of 2.18 eV in good agreement with previous measurements[21]. In contrast, dI/dV spectra acquired on the MTB showed distinct structure within the semiconducting bandgap (Fig. 1c). A high-resolution view of this spectrum around E_F (Fig. 2a) revealed an energy gap of 73 meV with sharp peaks at the band edges. The bandgap for each MTB was constant along its entire length, but we observed different gap sizes from MTB to MTB. Statistical analysis of 24 different MTBs at $T = 4.5$ K yields an average gap size of 100 meV with a standard deviation of 40 meV. The dI/dV spectrum also showed satellite peaks adjacent to both the occupied and unoccupied state band-edge peaks, offset by 14.2 ± 0.8 meV, independent of the particular bandgap. The dI/dV conductance maps measured at the satellite peak energies were modulated with the CDW period. We attribute these peaks to inelastic features in the STS spectra, related to lattice vibrations, but without a direct role in CDW formation.

To investigate the nature of the MTB bandgap, we studied the spatial distribution of the electronic band-edge states (Ψ_- and Ψ_+ in Fig. 2a) by measuring constant-height dI/dV conductance maps. Figure 2b shows representative dI/dV maps of the edge states below (Ψ_-) and above (Ψ_+) the gap, modulated at the CDW period. The occupied (blue) and unoccupied (red) state modulations were spatially out of phase, with nearly constant amplitude along the MTB (Fig. 2c). We can exclude drift-related artefacts between the two conductance maps, because they were simultaneously recorded by changing the bias between the forward and backward scan lines.

Owing to the finite length of $MoSe_2$ MTBs, the reported intensity modulations have been discussed in terms of quantum well states[5]. This cannot explain the LDOS features we observed (Fig. 2b), because MTBs as long as 30 nm showed uniform LDOS modulation, whereas the modulation amplitude should decay away from the ends of the MTB in the case of quantum confinement. Furthermore, we observed the same modulation periodicity for energies up to

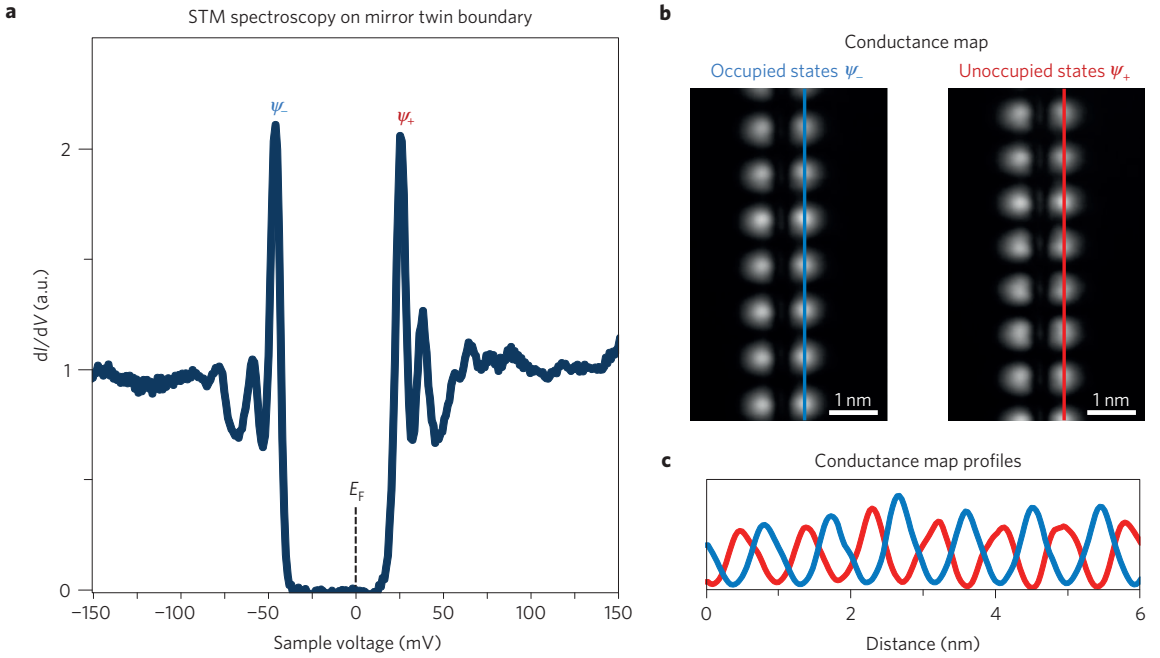

Figure 2 | Local density of states of mirror twin boundaries with an energy gap around the Fermi level. a, High-resolution STM dI/dV spectrum of a mirror twin boundary on monolayer $MoSe_2$/BLG showing an energy gap of 73 meV. 0 V sample voltage represents E_F. **b**, Representative dI/dV constant-height conductance maps recorded at voltages corresponding to edges states below (Ψ_-) and above (Ψ_+) the gap. Brighter regions indicate a larger DOS. **c**, Line profile of the dI/dV maps in **b** for occupied (blue) and empty (red) states, showing that the maxima for two states are spatially out of phase.

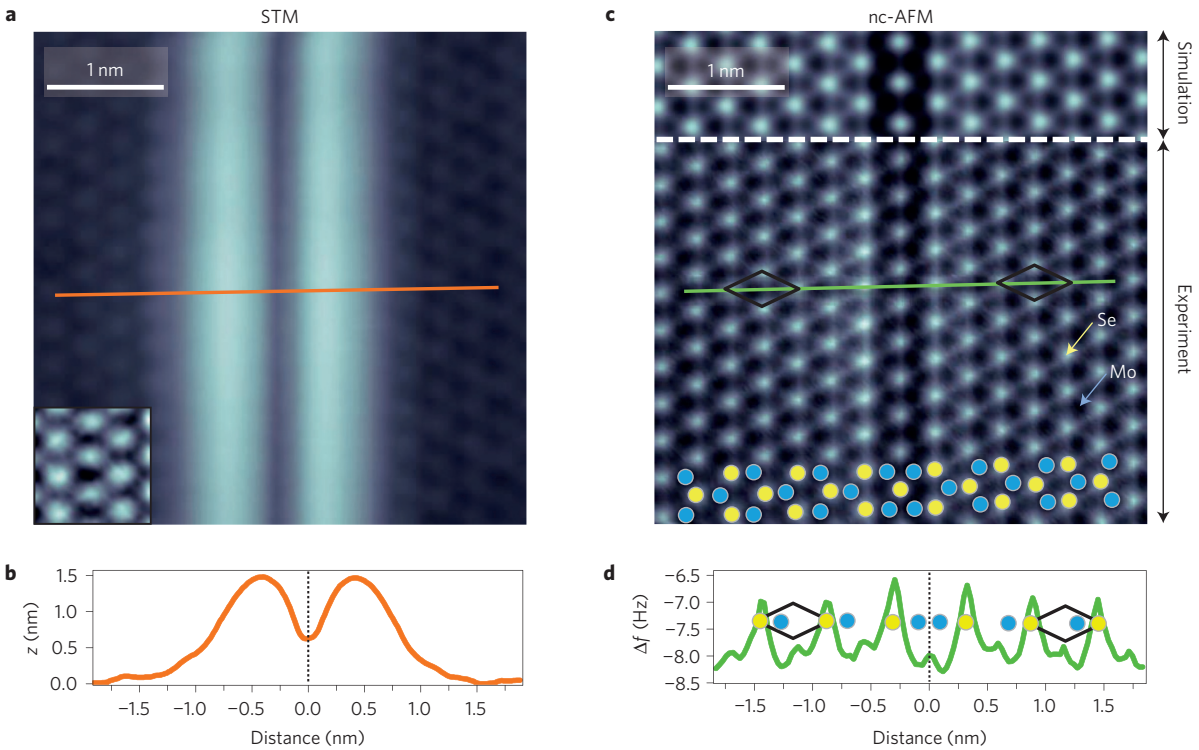

Figure 3 | Atomic resolution nc-AFM image of a mirror twin boundary reveals the precise atomic structure. a, STM topographic image of a mirror twin boundary in monolayer $MoSe_2$/BLG ($V_s = -1.5$ V, $I_t = 10$ pA, $T = 4.5$ K). Inset: small region of the main STM image away from the MTB, where the colour contrast has been adjusted to show the atomic lattice. **b**, Line profile through the STM image (orange line) showing the significant electronic contribution to the STM signal near the MTB. **c**, Nc-AFM image measured in same area and with the same CO-functionalized as **a**. Se (Mo) atom positions are indicated by yellow (blue) circles at the bottom of the figure. The Se atoms (bright areas, yellow) form an uninterrupted hexagonal lattice, whereas the Mo atoms (dark areas, blue) switch their positions within the indicated unit cells of the Se (black diamonds) between the two sides of the MTB. This assignment was corroborated by simulation of the frequency shift image (upper part of the figure above the white dashed line). **d**, Line profile of the nc-AFM image (green line) with the Se (yellow) and Mo (blue) atom positions overlaid, showing the mirror symmetry of the Mo lattice across the MTB.

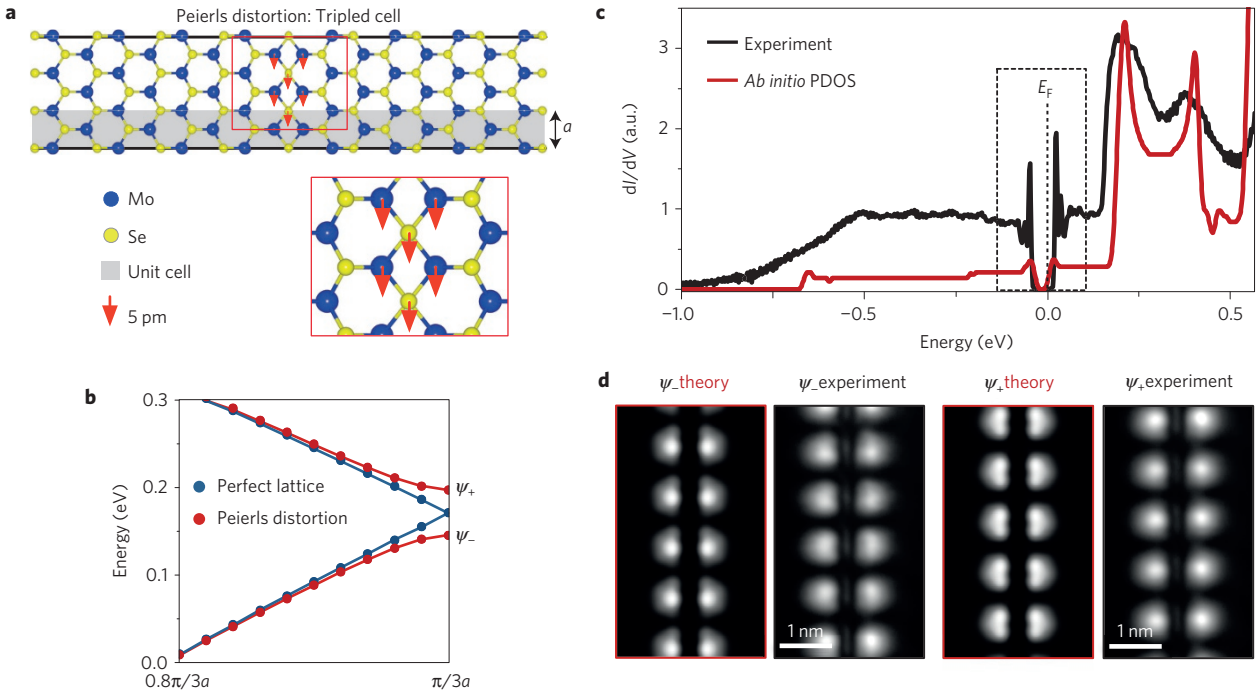

Figure 4 | Effect of a Peierls distortion on the electronic band structure of mirror twin boundaries in monolayer $MoSe_2$ from DFT calculations. **a**, Schematic of the tripled cell along the MTB (solid black lines). The unit cell along the MTB, with length *a*, is highlighted in grey. Red arrows indicate the induced distortions of the atomic positions near the MTB. An expanded view of the red-boxed regions is shown below. **b**, Calculated electronic band structure of the metallic state near the edge of the folded Brillouin zone ($\pi/3a$). It shows a gap opening when a Peierls distortion of 5 pm was introduced (red), whereas no gap exists for the undistorted system (blue). Note that the DFT gap opens at 0.175 eV above E_F (set to 0 eV). **c**, Projected density of states (PDOS) showing the gap opening when a Peierls distortion was introduced (red), along with the experimental STM d*I*/d*V* spectrum (grey). The calculated PDOS has been shifted by −0.175 eV to centre the gap at E_F (see text). **d**, Local DOS maps of the occupied (Ψ_-) and unoccupied (Ψ_+) states of the distorted MTB, showing out-of-phase modulations similar to the experimental conductance maps.

500 meV from the gap (Supplementary Fig. 6), whereas a quantum well would be expected to show wavelength dispersion.

We believe our STM images, spectra and conductance maps are best explained by charge density wave order intrinsic to MTBs in $MoSe_2$. Our conclusion follows from the fact that we observed a bandgap in an otherwise metallic electronic structure; a MTB contrast modulation period near three times the lattice constant; and occupied and unoccupied states at the bandgap that were spatially out of phase. These observations were independent of the substrate registry.

To further support this claim, we determined the atomic-scale morphology of the MTB. Although high-resolution STM images revealed the atomic structure of the $MoSe_2$ layer away from the MTB, electronic contributions dominated STM contrast near the line defect (Fig. 3a), making it impossible to resolve the MTB atomic structure by STM. Therefore, we performed nc-AFM using CO-functionalized tips[40] for enhanced spatial resolution. Because nc-AFM frequency shifts are not affected by the electronic structure near E_F, we could obtain atomically resolved images of the MTB. Figure 3c shows the nc-AFM frequency shift image taken at the same location and with the same tip as the STM image in Fig. 3a, unambiguously identifying the precise atomic geometry of the MTB.

We used the well-established atomic structure of $MoSe_2$ away from the MTB to interpret the nc-AFM image contrast. At the small tip–sample separation used here, brighter areas (higher frequency shifts) in nc-AFM images are generally due to short-range repulsive Pauli forces, whereas darker areas (lower frequency shifts) are due to long-range attractive van der Waals or electrostatic forces. Following this intuitive picture, we attribute the hexagonal lattice of bright features (yellow) to the higher-lying Se atoms, which were close enough to the tip to generate repulsive forces, and the dark features (blue) to the lower-lying Mo atoms, whose larger distance from the tip resulted in purely attractive forces. The MTB consisted of an atomic line of bright Se atoms surrounded by a region of attractive forces even stronger than in the unperturbed $MoSe_2$. We believe the stronger dark contrast is due to a higher density of Mo atoms, where each Se atom is bound to four Mo atoms instead of three. Simulations of the nc-AFM image contrast using previously established methods[41] (inset in the upper part of Fig. 3c) supported this structural model. The Se atoms form a continuous hexagonal lattice across the boundary, whereas the Mo atom positions are reflected across the single-atom-wide line defect (Fig. 3d), forming a mirror twin boundary[2–7]. All of the MTB structures we investigated were identical.

We computed the MTB electronic structure using DFT within the generalized gradient approximation of Perdew, Burke, and Ernzerhof (PBE)[42] using our MTB structural model and a simulation cell height of one unit cell along the MTB (grey area in Fig. 4a), similar to those used in previous work for both $MoSe_2$[2] and MoS_2[3,7]. Our DFT calculations found a metallic band originating from states in the MTB, which crossed E_F about one third of the way along the Γ–X Brillouin zone direction. This band was absent in calculations of pristine monolayer $MoSe_2$ (Supplementary Fig. 4b). Inclusion of spin–orbit coupling did not substantially modify the DFT band structure, although a degeneracy of states around the midpoint of the Brillouin zone was lifted (Supplementary Fig. 4c). The significant dispersion of the metallic band, combined with the in-plane screening from outside the MTB region and from the substrate, suggest that electron–electron interactions are not responsible for the CDW ordering observed here.

CDW order can result from a Peierls instability[31], where a periodic lattice distortion opens a gap at E_F, reducing the total

energy of the system, and leading to a charge density modulation with a period that reflects the lattice distortion. Because the experimentally observed charge density modulation was three times the lattice constant within measurement precision, we tripled the size of our DFT simulation cell along the MTB (Fig. 4a). Relaxing the DFT geometry did not lead to a spontaneous Peierls distortion and CDW formation. This was not unexpected because the calculated metallic state did not cross E_F at exactly one third of the Brillouin zone size. As a result, such a Peierls distortion will not lower the calculated total energy of the system, because only a small part of the band structure is modified (Supplementary Fig. 5d) above E_F near the edge of the folded Brillouin zone.

To theoretically explore the effects of Peierls distortions on the MTB electronic structure, we introduced lattice distortions along the MTB with the periodicity of the enlarged simulation cell. Figure 4a illustrates one such distortion, where the red arrows indicate displacements of 5 pm along the line defect. As shown in Fig. 4b, this opened a 50 meV bandgap at the edge of the folded Brillouin zone. Not surprisingly, the gap did not open exactly at E_F, because the metallic band computed with DFT-PBE for the undistorted MTB in the tripled cell does not cross E_F exactly at the edge of the folded Brillouin zone. Instead, the calculated gap opened 0.175 eV above E_F. After aligning the bandgaps in our calculated DOS and our measured dI/dV spectrum (Fig. 4c), we found excellent agreement between experiment and theory, including features as far away as 0.5 eV from E_F. Moreover, the spatial distribution of the computed LDOS perfectly reproduces the experimental maps (Fig. 4d): the calculated Ψ_- (Ψ_+) states below (above) the gap are seen to exhibit the same shape, periodicity and spatial phase shift as observed in our measurements.

From our calculations, we found that different types of distortions with tripled periodicity along the MTB led to qualitatively similar gaps near the edge of the folded Brillouin zone. Crucially, our calculations showed that distortions with doubled periodicity did not result in gap formation (Supplementary Fig. 5a,c). Furthermore, we found that the magnitude of the calculated gap was linear with the lattice distortion amplitude we introduced, consistent with the expected behaviour of a CDW associated with a Peierls distortion[43]. This may explain experimentally observed variations in the gap size between MTBs. Both the strain inherent to MTBs, as well as local strains in the adjacent $MoSe_2$ twin domains (Supplementary Fig. 3), could influence the magnitude of the distortion.

Although introducing a Peierls distortion of just 5 pm was sufficient to reproduce the observed CDW electronic structure, we note that this would be below the spatial resolution of our nc-AFM measurements. In addition, because DFT-PBE calculations are well known to underestimate bandgaps, we expect that the true gap would be slightly larger than predicted here. The fact that an induced MTB lattice distortion with tripled periodicity opened a gap near E_F, and that the calculated LDOS agrees well with both the experimental dI/dV curves and the spatially resolved conductance maps, together provide strong support for the existence of one-dimensional CDW order intrinsic to $MoSe_2$ MTBs.

In conclusion, we observed the formation of one-dimensional charge density waves along MTBs in $MoSe_2$, fully characterized by combined STS/nc-AFM measurements, and supported by DFT calculations. The $MoSe_2$ MTB illustrates how hierarchical defects can add functionality to 2D TMDs, and specifically provides an exceptional model to study the physics of symmetry breaking in one-dimensional correlated systems. It presents new opportunities to study the charge transport in such systems, including Fröhlich conduction, as well as the effects of pinning due to point defects or adatoms, and confinement due to intersections between macroscopically interconnected CDWs within a one-dimensional network.

Methods

Methods and any associated references are available in the online version of the paper.

Received 17 November 2015; accepted 11 March 2016; published online 18 April 2016

References

1. van der Zande, A. M. *et al*. Grains and grain boundaries in highly crystalline monolayer molybdenum disulphide. *Nature Mater.* **12,** 554–561 (2013).
2. Lehtinen, O. *et al*. Atomic scale microstructure and properties of Se-deficient two-dimensional $MoSe_2$. *ACS Nano* **9,** 3274–3283 (2015).
3. Zou, X., Liu, Y. & Yakobson, B. I. Predicting dislocations and grain boundaries in two-dimensional metal-disulfides from the first principles. *Nano Lett.* **13,** 253–258 (2013).
4. Zhou, W. *et al*. Intrinsic structural defects in monolayer molybdenum disulfide. *Nano Lett.* **13,** 2615–2622 (2013).
5. Liu, H. *et al*. Dense network of one-dimensional midgap metallic modes in monolayer $MoSe_2$ and their spatial undulations. *Phys. Rev. Lett.* **113,** 066105 (2014).
6. Gibertini, M. & Marzari, N. Emergence of one-dimensional wires of free carriers in transition-metal-dichalcogenide nanostructures. *Nano Lett.* **15,** 6229–6238 (2015).
7. Le, D. & Rahman, T. S. Joined edges in MoS_2: metallic and half-metallic wires. *J. Phys. Condens. Matter* **25,** 312201 (2013).
8. Lahiri, J. *et al*. An extended defect in graphene as a metallic wire. *Nature Nanotech.* **5,** 326–329 (2010).
9. Yazyev, O. V. & Louie, S. G. Electronic transport in polycrystalline graphene. *Nature Mater.* **9,** 806–809 (2010).
10. Ugeda, M. M., Brihuega, I., Guinea, F. & Gómez-Rodríguez, J. M. Missing atom as a source of carbon magnetism. *Phys. Rev. Lett.* **104,** 096804 (2010).
11. Tsen, A. W. *et al*. Tailoring electrical transport across grain boundaries in polycrystalline graphene. *Science* **336,** 1143–1146 (2012).
12. López-Polín, G. *et al*. Increasing the elastic modulus of graphene by controlled defect creation. *Nature Phys.* **11,** 26–31 (2015).
13. Mak, K. F., Lee, C., Hone, J., Shan, J. & Heinz, T. F. Atomically thin MoS_2: a new direct-gap semiconductor. *Phys. Rev. Lett.* **105,** 136805 (2010).
14. Splendiani, A. *et al*. Emerging photoluminescence in monolayer MoS_2. *Nano Lett.* **10,** 1271–1275 (2010).
15. Zhang, Y. *et al*. Direct observation of the transition from indirect to direct bandgap in atomically thin epitaxial $MoSe_2$. *Nature Nanotech.* **9,** 111–115 (2014).
16. Baugher, B. W. H., Churchill, H. O. H., Yang, Y. & Jarillo-Herrero, P. Intrinsic electronic transport properties of high-quality monolayer and bilayer MoS_2. *Nano Lett.* **13,** 4212–4216 (2013).
17. Kang, K. *et al*. High-mobility three-atom-thick semiconducting films with wafer-scale homogeneity. *Nature* **520,** 656–660 (2015).
18. Qiu, D. Y., da Jornada, F. H. & Louie, S. G. Optical spectrum of MoS_2: many-body effects and diversity of exciton states. *Phys. Rev. Lett.* **111,** 216805 (2013).
19. Bernardi, M., Palummo, M. & Grossman, J. C. Extraordinary sunlight absorption and one nanometer thick photovoltaics using two-dimensional monolayer materials. *Nano Lett.* **13,** 3664–3670 (2013).
20. Britnell, L. *et al*. Strong light–matter interactions in heterostructures of atomically thin films. *Science* **340,** 1311–1314 (2013).
21. Ugeda, M. M. *et al*. Giant bandgap renormalization and excitonic effects in a monolayer transition metal dichalcogenide semiconductor. *Nature Mater.* **13,** 1091–1095 (2014).
22. Geim, A. K. & Grigorieva, I. V. Van der Waals heterostructures. *Nature* **499,** 419–425 (2013).
23. Lee, C.-H. *et al*. Atomically thin p–n junctions with van der Waals heterointerfaces. *Nature Nanotech.* **9,** 676–681 (2014).
24. Qiu, H. *et al*. Hopping transport through defect-induced localized states in molybdenum disulphide. *Nature Commun.* **4,** 2642 (2013).
25. Cai, L. *et al*. Vacancy-induced ferromagnetism of MoS_2 nanosheets. *J. Am. Chem. Soc.* **137,** 2622–2627 (2015).
26. Bao, W. *et al*. Visualizing nanoscale excitonic relaxation properties of disordered edges and grain boundaries in monolayer molybdenum disulfide. *Nature Commun.* **6,** 7993 (2015).
27. Zhang, Z., Zou, X., Crespi, V. H. & Yakobson, B. I. Intrinsic magnetism of grain boundaries in two-dimensional metal dichalcogenides. *ACS Nano* **7,** 10475–10481 (2013).
28. Lauritsen, J. V. *et al*. Hydrodesulfurization reaction pathways on MoS_2 nanoclusters revealed by scanning tunneling microscopy. *J. Catal.* **224,** 94–106 (2004).

29. Jaramillo, T. F. *et al*. Identification of active edge sites for electrochemical H_2 evolution from MoS_2 nanocatalysts. *Science* **317,** 100–102 (2007).
30. Grüner, G. *Density Waves in Solids* (Perseus, 2000).
31. Peierls, R. E. *Quantum Theory of Solids* (Oxford Univ. Press, 1955).
32. Peng, J.-P. *et al*. Molecular beam epitaxy growth and scanning tunneling microscopy study of $TiSe_2$ ultrathin films. *Phys. Rev. B* **91,** 121113 (2015).
33. Ugeda, M. M. *et al*. Characterization of collective ground states in single-layer $NbSe_2$. *Nature Phys.* **12,** 92–97 (2016).
34. Heeger, A. J., Kivelson, S., Schrieffer, J. R. & Su, W.-P. Solitons in conducting polymers. *Rev. Mod. Phys.* **60,** 781–850 (1988).
35. Yeom, H. W. *et al*. Instability and charge density wave of metallic quantum chains on a silicon surface. *Phys. Rev. Lett.* **82,** 4898–4901 (1999).
36. Jérome, D. Organic conductors: from charge density wave TTF-TCNQ to superconducting $(TMTSF)_2PF_6$. *Chem. Rev.* **104,** 5565–5591 (2004).
37. Shin, J. S., Ryang, K.-D. & Yeom, H. W. Finite-length charge-density waves on terminated atomic wires. *Phys. Rev. B* **85,** 073401 (2012).
38. Cheon, S., Kim, T.-H., Lee, S.-H. & Yeom, H. W. Chiral solitons in a coupled double Peierls chain. *Science* **350,** 182–185 (2015).
39. Murata, H. & Koma, A. Modulated STM images of ultrathin $MoSe_2$ films grown on MoS_2(0001) studied by STM/STS. *Phys. Rev. B* **59,** 10327–10334 (1999).
40. Gross, L., Mohn, F., Moll, N., Liljeroth, P. & Meyer, G. The chemical structure of a molecule resolved by atomic force microscopy. *Science* **325,** 1110–1114 (2009).
41. Hapala, P. *et al*. Mechanism of high-resolution STM/AFM imaging with functionalized tips. *Phys. Rev. B* **90,** 085421 (2014).
42. Perdew, J. P., Burke, K. & Ernzerhof, M. Generalized gradient approximation made simple. *Phys. Rev. Lett.* **77,** 3865–3868 (1996).
43. Grüner, G. The dynamics of charge-density waves. *Rev. Mod. Phys.* **60,** 1129–1181 (1988).

Acknowledgements

We acknowledge P. Hapala for assistance with the nc-AFM image simulations. We thank our colleagues at the Molecular Foundry for stimulating discussion and assistance. Work at the Molecular Foundry was supported by the Office of Science, Office of Basic Energy Sciences, of the US Department of Energy under Contract No. DE-AC02-05CH11231 (user proposal #3282) (STM imaging, STM spectroscopy, theoretical simulations, and analysis). A.W.-B. and S.W. were supported by the US Department of Energy, Office of Science, Basic Energy Sciences, Scientific User Facilities Division (NSRCs) Early Career Award. S.B. acknowledges fellowship support by the European Union under FP7-PEOPLE-2012-IOF-327581. ALS and SIMES were supported by Office of Basic Energy Science, US DOE, under contract numbers DE-AC02-05CH11231 and DE-AC02-76SF00515, respectively. H.R. acknowledges support from the Max Planck Korea/POSTECH Research Initiative of the NRF under Project No. NRF-2011-0031558. M.B.S. was supported by the Division of Materials Science and Engineering through the Chemical and Mechanical Properties of Surfaces and Interfaces Program. Portions of the computational work were done with NERSC resources. M.F.C. acknowledges support from National Science Foundation grant EFMA-1542741 (sample surface preparation development).

Author contributions

S.B., S.W. and A.W.-B. conceived the work and designed the research strategy. S.B. and S.W. measured and analysed the STM/STS and nc-AFM data. Z.-F.L. performed the theoretical calculations. Y.Z. and H.R. performed the MBE growth and characterization of the samples. S.-K.M., Z.H. and Z.-X.S. supervised the MBE growth and sample characterization. J.B.N. supervised the theoretical calculations. M.M.U., E.W., M.B.S., F.W., M.F.C. and D.F.O. participated in the acquisition and interpretation of the experimental data. A.W.-B. supervised the STM/STS and nc-AFM measurements. S.B. wrote the manuscript with help from S.W., Z.-F.L., D.F.O., J.B.N. and A.W.-B. All authors contributed to the scientific discussion and manuscript revisions.

Additional information

Supplementary information is available in the online version of the paper. Reprints and permissions information is available online at www.nature.com/reprints. Correspondence and requests for materials should be addressed to S.B., D.F.O. or A.W.-B.

Competing financial interests

The authors declare no competing financial interests.

Methods

The experiments were carried out on high-quality single layers of $MoSe_2$ grown by molecular beam epitaxy on epitaxial bilayer graphene (BLG) on 6H-SiC(0001). The structural quality and the coverage of the submonolayer $MoSe_2$ samples were characterized by *in situ* reflection high-energy electron diffraction (RHEED), low-energy electron diffraction (LEED) and core-level photoemission spectroscopy (PES) at the HERS endstation of beamline 10.0.1, Advance Light Source, Lawrence Berkeley National Laboratory[21].

STM/nc-AFM imaging and STS measurements were performed at $T = 4.5$ K in a commercial Createc ultrahigh vacuum (UHV) system equipped with an STM/qPlus sensor. The modulation period varied slightly from MTB to MTB. The average periodicity was measured to be 0.98 ± 0.05 nm (2.99 ± 0.15 lattice constants) over 56 different MTB using the simultaneously resolved $MoSe_2$ lattice and taking the lattice parameter to be $a_0 = 0.329$ nm (errors are given by the standard deviation). STS differential conductance (dI/dV) point spectra and spatial maps were measured in constant-height mode using standard lock-in techniques ($f = 775$ Hz, $V_{r.m.s.} = 2.1$ mV, $T = 4.5$ K). dI/dV spectra from Au(111) were used as an STS reference to control tip quality. The averaged experimental bandgap ($100 \text{ mV} \pm 40 \text{ mV}$) was obtained by statistical analysis of 24 different MTBs on several samples and using different tip preparations (error is given by the standard deviation). Bandgap widths were measured from peak to peak. Nc-AFM images were recorded by measuring the frequency shift of the qPlus resonator (sensor frequency $f_0 \approx 30$ kHz, $Q \approx 25{,}000$) in constant-height mode with an oscillation amplitude of 180 pm. Nc-AFM images were measured at a sample bias $V_s = -50$ mV, using a tip functionalized with a single CO molecule[40]. STM/STS data were analysed and rendered using WSxM software[44].

DFT calculations were performed with the generalized gradient approximation of PBE[42] using the Vienna Ab initio Simulation Package (VASP)[45], which makes use of a plane-wave basis and projector augmented-wave pseudopotentials with a plane-wave cutoff of 225 eV. We imposed periodic boundary conditions along the MTB direction, and added 10 Å of vacuum on each side of the structure along the other two directions. The supercell lattice parameter was 3.33 Å along the MTB direction, equivalent to the optimized DFT-PBE lattice constant for one-layer $MoSe_2$, and was 66.14 Å and 23.32 Å, respectively, along the other two directions. The atomic positions were optimized until the Hellmann–Feynman force on each atom was less than 0.04 eV $Å^{-1}$. A $1 \times 18 \times 1$ k-mesh was used in the relaxation of the unit cell structure, with 18 k-points sampled along the MTB direction. All electronic structure calculations were performed using optimized geometries and were converged with respect to the length of the structure perpendicular to the MTB direction. The CDW electronic structure was calculated using a $1 \times 18 \times 1$ k-mesh for the unit cell, and a $1 \times 6 \times 1$ k-mesh for the supercell containing three unit cells. Non-spin-polarized calculations were performed, as it has been shown that this particular type of MTB structure[7] is not spin polarized. We found that inclusion of spin–orbit interactions did not qualitatively change the band structure. The band structure was calculated using 51 k-points sampled along the MTB direction.

References

44. Horcas, I. *et al*. WSXM: a software for scanning probe microscopy and a tool for nanotechnology. *Rev. Sci. Instrum.* **78,** 013705 (2007).
45. Kresse, G. & Furthmüller, J. Efficient iterative schemes for *ab initio* total-energy calculations using a plane-wave basis set. *Phys. Rev. B* **54,** 11169–11186 (1996).